Studies in Surface Science and Catalysis 143
E. Gaigneaux et al. (Editors)



# Preparation of Ce-Zr-O composites by a polymerized complex method

T. G. Kuznetsova, V. A. Sadykov, E. M. Moroz, S. N. Trukhan, E. A. Paukshtis, V. N. Kolomiichuk, E. B. Burgina, V. I. Zaikovskii, M. A. Fedotov, V. V. Lunin,* E. Kemnitz**.

Boreskov Institute of Catalysis, SB RAS, Lavrentieva 5, Novosibirsk 630090, Russia

* - Chemical Department of Lomonosov Moscow State University, Moscow, Russia

** - Institute for Chemistry, Humboldt -Univ., Berlin, Germany.

Fluorite-like oxides based on $CeO_2$ and $ZrO_2$ and Ca and/or F-modified have been prepared by organic polymerized complex method. Dispersed phase-pure cubic fluorite-like mixed oxide phases were obtained provided the synthesis parameters are optimized. The real/defect structure of those phases is characterized by using combination of diffraction and spectroscopic methods. For bulk structure, the main feature is the presence of strong framework distortions due to complex defects including extended ones generated by guest cations and/or anions. For ceria-based solid solutions, the nature of surface Brönsted and Lewis acid centers, their density and ability to stabilize charged molecular forms of oxygen strongly depend upon the sample composition and preparation route, surface being in general more disordered compared with pure ceria phase.

## 1. INTRODUCTION

Ce-Zr-O solid solutions are important components of promising catalysts for different oxidative processes, in particular, for partial methane oxidation into syngas and three-way car exhaust clean-up [1-2]. Different synthesis procedures have been used for the preparation of Ce-Zr-O solid solutions including sintering of oxides, coprecipitation of mixed hydroxides from nitrate salts, decomposition of mixed acetates or citrates [3-5]. Homogeneous metastable tetragonal solid solutions were also successfully synthesized by the organic polymerized complex method (OPCM) which is a modified version of the polymeric precursor method suggested by Pechini [5].

In this work OPCM was further modified for the preparation of highly dispersed fluorite-like oxide systems including $CeO_2$, Ce-Zr-O solid solutions and partially stabilized zirconias. The aim of the work was to elucidate the effect of the samples composition and specificity of their preparation procedure on the bulk and surface defect structure, which is known to be of importance for catalysis of red-ox reactions.

## 2. EXPERIMENTAL

Water solutions (WS) of starting salts (nitrates of Ce, Y, Ca; oxychloride of zirconium, ammonium and calcium fluorides) or their solid crystalline hydrates (SCH) (the content of admixed rare earth cations was less than 0.2 wt. %) taken in a required ratio were added at 60 °C to the solution of citric acid in ethylene glycol (1:4 mole ratio) while the Me: citric acid (CA) ratio was varied from Me:CA=1:2 to 1:10. Solutions were heated up to 140 °C for the time required to form a highly viscous polymeric brownish gel. This product was further calcined in air up to 700 °C. The degree of oxygen substitution for fluorine was less than 20 at. % or 40 at. % in samples of Ce-Zr series or Ce-Zr-Ca series. Some calcined samples were fluorinated by heating with solid $NH_4F$ at 220°Ñ for 6 h followed by annealing at 500°Ñ for 1 h. $CeO_2$ samples were prepared through the OPCM route and by $Ce^{3+}$ nitrate decomposition at 700 °C.

The X-ray phase analysis of samples was carried out using a HZG-4C diffractometer (Cu $K_\alpha$ radiation and a flat monochromator) in the range of 2θ angles equal to 1-70°. The unit cell parameter of ceria and modified composites was determined from the position of 311 diffraction peak.

The surface chemical composition was analyzed with SIMS method using a MS-7201 mass-spectrometer. The energy of the incident $Ar^+$ ion beam was equal to 4 Kev, the current density 10-20 mka/cm$^2$. To prevent sample charging during ion bombardment, samples were supported onto high purity indium foil.

Static magnetic susceptibility was measured by the Faraday method. Infra-red spectra of samples in the 220-4000 cm$^{-1}$ range were recorded using a BOMEN M 102 spectrometer. UV-Vis spectra were recorded using a Shimadzu 8300 spectrometer equipped with a diffuse scattering DRS 8000 cell. Spectra were recorded in the 10000-60000 cm$^{-1}$ range with 4 cm$^{-1}$ resolution, the number of scans being equal to 50. Samples were loaded into the vacuum cells equipped with $CaF_2$ windows. To decrease the mirror reflection, a sample layer was inclined for 20-25% with respect to the horizontal plane.

The surface properties were probed by the IR spectroscopy of adsorbed CO and $O_2$ test molecules (a Fourier-transform IFS 113V Bruker spectrometer). In these experiments, samples were pressed in wafers with densities 4.4-22.7 mg/cm$^2$ and pretreated in the IR cell first at 100 Torr of $O_2$ and then in vacuum at 400 °C for 1 h. CO was adsorbed at 77 K first by introducing several doses (each CO dose corresponds to ≈ 4 μmol), finally setting CO pressure to 10 Torr. $O_2$ (20 Torr) was adsorbed at RT. The data were presented as absorbance normalized to the unit weight of sample.

## 3. RESULTS AND DISCUSSION

### 3.1. Phase composition

Table 1 lists data for the phase composition and specific surface area of samples prepared and studied here. For pure ceria samples prepared either via nitrate salt decomposition, or OPCM route, the cubic fluorite phase with the lattice parameter **a**= 5.411 Å corresponding to a standard data (JCPDS 43-1002) was revealed. Samples prepared via OPCM route possess higher specific surface areas increasing with the content of CA.

Table 1
XRD data of $CeO_2$, $ZrO_2$ and Ce-Zr-O based composites.

| No | Chemical composition | Preparation route | Spec. Surf. area, $m^2/g$ | Phase composition (cell parameter, Å) |
|---|---|---|---|---|
| 1 | $CeO_2$ | $Ce^{3+}$ nitrate decomposition | 3 | $CeO_2$ (5.411) |
| 2 | | OPCM (SCH - Me : CA=1 : 2) | 6 | $CeO_2$ (5.411) |
| 3 | | OPCM (WS - Me : CA=1 : 6) | 19 | $CeO_2$ (5.411) |
| 4 | $Ce_{0.8}Zr_{0.2}O_x$ | OPCM (SCH - Me : CA=1 : 2) | 22 | $CeO_2$ (5.380) |
| 5 | | OPCM (WS - Me : CA=1 : 2) | 24 | $CeO_2$ (5.376) |
| 6 | | OPCM (WS - Me : CA=1 : 6) | 33 | $CeO_2$ (5.368) |
| 7 | | OPCM (WS - Me : CA=1 : 10) | 39 | $CeO_2$ (5.368) |
| 8 | $Ce_{0.8}Zr_{0.2}O_xF_y$ | OPCM (SCH - Me : C 1 : 2); GpF | 20 | $CeO_2$ ( 5.383); $CeF_3$, $ZrO_2^C$*, |
| 9 | | OPCM (SCH - Me : CA=1 : 2) - $NH_4F$ | 11 | $CeO_2$ (5.384) |
| 10 | $Ce_{0.5}Zr_{0.5}O_x$ | OPCM (SCH - Me : CA=1 : 2 | 16 | $CeO_2$ (5.385), $ZrO_2^C$ (5.139) |
| 11 | | OPCM (WS - Me : CA=1 : 6) | 69 | $CeO_2$ (5.282) |
| 12 | $Ce_{0.5}Zr_{0.5}O_xF_y$ | OPCM (SCH - Me : CA=1 : 2) - $NH_4F$ | 31 | $CeO_2$ (5.274 ), $ZrO_2^C$* |
| 13 | $Ce_{0.6}Zr_{0.2}Ca_{0.2}O_x$ | OPCM (SCH - Me : CA=1 : 2 | 54 | $CeO_2$ (5.368 ), $ZrO_2^C$ ( 5.134 ); |
| 14 | | OPCM (WS - Me : CA=1 : 6) | 44 | $CeO_2$ ( 5.358 ) |
| 15 | $Ce_{0.6}Zr_{0.2}Ca_{0.2}O_xF_y$ | OPCM (SCH - Me : CA=1 : 2) - $CaF_2$ | 15 | $CeO_2$ ( 5.383 ), $ZrO_2^C$ ( 5.152 ), $CaF_2$ |
| 16 | | OPCM (WS - Me : CA=1 : 6) - $NH_4F$ | 58 | $CeO_2$ ( 5.358 ) |
| 17 | $Zr_{0.9}Ca_{0.1}O_x$ | OPCM (WS - Me : CA=1 : 6) | 60 | $ZrO_2^C$ ( 5.121) |
| 18 | $Zr_{0.8}Ce_{0.1}Y_{0.1}O_x$ | OPCM (WS - Me : CA=1 : 6) | 90 | $ZrO_2^C$ ( 5.152) |
| 19 | $ZrO_2$ | OPCM (WS - Me : CA=1 : 6) | 8 | $ZrO_2^M$, $ZrO_2^T$ |

OPCM - organic polymerized complex method; SCH - solid crystalline hydrates; WS - water solutions; Me : CA - metal : citric acid ratio; GpF-gas-phase fluorination ; $ZrO_2^C$ - cubic phase, $ZrO_2^M$ - monoclinic phase, $ZrO_2^T$ - tetragonal phase; * - trace of cubic phase.

When water salts solutions are used in OPCM synthesis, provided the Me:CA ratio is equal to 1:6 in all the composition range studied here (up to Zr relative content equal to 0.9), single phase samples with a cubic fluorite-like structure are formed. Thus, for ceria-zirconia samples with zirconia content up to 50 mol. %, ceria-based cubic solid solution is formed. For those samples, the lattice parameter is decreased as compared with that of a pure ceria phase, due to cerium cations substitution by zirconium cations with a smaller

cation radius (0.88 Å and 0.82 Å, respectively). For single-phase binary samples containing 20 and 50 mol. % of $ZrO_2$, the lattice parameter **a** is equal, respectively, to 5.368 Å and 5.282 Å, which is somewhat higher than additive values of 5.35 Å è 5.25 Å expected for the ideal solid solutions of cubic ceria and zirconia with the lattice parameters taken to be equal to 5.411 Å è 5.090 Å (JCPDS 42-1164), respectively.

For samples prepared by using a mixture of solid crystalline hydrates with Me:CA ratio equal to 1:2, deviations from the additivity are even bigger, though in this case, part of zirconium is segregated as a separate zirconia phase.

Gas phase fluorination of mixed Ce-Zr oxides is accompanied by a partial decomposition of the solid solution, leading to the segregation of $CeF_3$ (JCPDS 08-0045) and $ZrO_2$ phases. More or less homogeneous fluorine-modified solid solutions are obtained when ammonium fluoride is added to the mixed solution of the starting compounds. In general, the effect of fluorine on the lattice parameter depends upon the zirconium and/or calcium content and degree of precursors mixing in the course of synthesis (Table 1). Thus, when a mixture of solid crystalline hydrates is used, the effect of fluorine is more pronounced in systems with a higher (50 mol. %) content of zirconium. When fluorine is introduced into Ce-Zr-Ca-O solid solution, its lattice parameter is not noticeably affected.

### 3.2. Bulk structure

Deviation of lattice parameters of homogeneous cubic solid solutions from the additive values could be assigned either to the presence of $Ce^{3+}$ cations with a bigger ionic radius, or to distortions of the lattice due to incorporation of guest cations/anions. Magnetic susceptibility data ($\chi_{298}$ is in the range of -0.31÷+1.2, $10^{-6}$ CGSM units) indicate that the relative content of $Ce^{3+}$ cations does not exceed 1 %. A small content of those cations implies that their effect on the lattice parameters has to be negligible. Hence, some distortions appear to be responsible for the relative lattice expansion considered here.

In general, the lattice distortion can be caused both by point and extended defects generated due to incorporation of modifying cations (Zr, Ca) or anions (fluorine, residual lattice hydroxyls). Extended defects differing from the surrounding lattice by the electron density can be detected by using SAXS [6], while point defects (anion vacancies etc) are usually probed by UV-Vis [7].

The integral intensity of X-ray scattering on the extended regions with modified electron density (typical sizes up to 200 Å) is listed in Table 2. The relative density of extended defects strongly depends upon the samples composition and their preparation route. Moreover, the size distribution of those defects varies as well. Thus, for pure ceria, extended defects with typical sizes in the range of 20-40 Å dominate. Since increasing water content in polymerized precursor increases the integral intensity of scattering, for pure ceria extended defects can be tentatively assigned to microstrains generated by the presence of residual hydroxyls in the lattice (vide infra). Along with those defects, more extended defect regions (typical sizes up to 80-170 Å) were detected as well. Those defects are usually assigned to intergrain boundaries present in samples with relatively big particle sizes [6].

When up to 20 mol. % of zirconia are added, the size distribution of inhomogeneities changes rather slightly, the share of more extended defects being decreased. Since integral density of scattering for ceria-zirconia samples with a low Zr

content strongly depends upon the mode of reagents premixing before adding to citric acid-ethylene glycol solution, namely, higher integral intensity is observed for less homogeneous samples, it implies that in the case of a poor reagent mixing, a part of extended defects is generated by the incorporated zirconium cations probably present as clusters or microinclusions.

When fluorine is incorporated into a sample with a low zirconium content, the integral density of extended defects remains nearly constant, although the relative share of defects assigned to intergrain boundaries somewhat increases.

For samples with a relatively high content of zirconium characterized by a higher dispersion (higher specific surface area, Table 1), extended defects in the range of 10-25 Å dominate. Those defects can be tentatively assigned to the lattice distortion around incorporated guest cations/anions with associated local charge variation as detected by photoemission and XANES studies [8]. The integral density of those clustered defects tends to increase with addition of zirconium and fluorine. On the contrary, for calcium-containing samples, the density of those extended defects appears to be lower.

FTIRS data of lattice modes (not shown for brevity) revealed pronounced distortion of the local coordination sphere of cations in samples synthesized via OPCM route. In ceria samples, along with main band at ~ 400 $cm^{-1}$, a strong shoulder at ~ 510 $cm^{-1}$ is observed as well, which is not expected for symmetric cubic phase. This feature can be assigned to the coordination sphere distortion due to the presence of residual hydroxyls. In ceria-zirconia samples the intensity of this high-frequency shoulder is increased, while the band is broaden. Since in cubic Ca-$ZrO_2$ sample prepared via OPCM route (Table 1), a band at ~ 505 $cm^{-1}$ with a strong shoulder at ~ 590 $cm^{-1}$ is observed, it implies that a similar type of Zr cations coordination exists in $CeO_2$-$ZrO_2$ samples, which agrees with the conclusions of Liu et al [8].

Fig. 1 shows UV-Vis spectra of pure ceria and zirconia phases as well as those of fluorite-like solid solutions with a homogeneous distribution of components. For pure ceria and zirconia samples the spectra differ substantially due to the difference of those oxides band gap width equal to 3.1 and 5.0 eV, respectively. Incorporation of Zr into the framework of ceria is accompanied by the appearance of an absorption in the visible range (12000-25000 $cm^{-1}$), which increases with the content of zirconium. This absorption can be assigned to $Ce^{3+}$ cations characterized by absorption band at ~ 15000 $cm^{-1}$ [9], and/or to F and V centers such as those revealed in pure zirconia [10]. For samples modified by Ca or Ca + F, the enhanced absorption in the range of 26000-40000 $cm^{-1}$ can be assigned to bulk/surface peroxide groups $O_2^{2-}$ [11]. In the visible range, calcium incorporation increases the absorption apparently due to the generation of anion vacancies. Since the simultaneous incorporation of calcium and fluorine decreases absorption in this range, it implies that anion vacancies are filled by fluorine anions.

Table 2.
SAXS integral intensity I (a.u) and maxima position of Ce-Zr based composites prepared from solid crystalline hydrates (a) and water solutions of salts (Me : CA=1 : 6) (b).

| Chemical composition | I (a.u.)/maxima position, Å | |
|---|---|---|
| | a | b |
| $CeO_2$ | 32/20-40$^s$, 80-170$^m$ | 164/20-40$^s$, 80-170$^w$ |
| $Ce_{0.8}Zr_{0.2}O_x$ | 142/20-40$^s$, 80-170$^w$ | 35/20-40$^s$, 80-170$^w$ |
| $Ce_{0.8}Zr_{0.2}O_xF_y$ | 135/35-55$^s$, 80-170$^m$ | - |
| $Ce_{0.5}Zr_{0.5}O_x$ | 335/10-25$^s$, 40-60$^w$ | 378/10-25$^s$, 40-60$^w$ |
| $Ce_{0.5}Zr_{0.5}O_xF_y$ | 717/10-25$^s$, 40-60$^w$ | - |
| $Ce_{0.6}Zr_{0.2}Ca_{0.2}O_x$ | 155/10-25$^s$, 40-60$^w$ | 66/10-25$^s$, 40-60$^w$ |
| $Ce_{0.6}Zr_{0.2}Ca_{0.2}O_xF_y$ | 82/10-25$^s$, 40-60 | 323/10-25, 40-60$^w$ |
| $Ce_{0.1}Y_{0.1}Zr_{0.8}O_x$ | - | 1088/10-25$^s$, 40-60$^s$ |

s - strong, m - medium, w - weak - contribution of intensity.

### 3.3. Surface properties

According to SIMS data (not shown here for brevity), zirconium cations and fluorine anions are rather uniformly distributed across the particle depths, while calcium tends to segregate at the surface, where its content is up to several times higher than in the bulk.

TEM data (not shown for brevity) revealed the samples particles to be of a platelet appearance, with the most developed faces being of (111) and (110) types as determined by SED analysis. Intergrain boundaries are present in low surface area samples.

In the spectra of CO adsorbed at 77 K on the surface of samples pretreated in oxygen, at low CO coverages (Fig. 2a), bands corresponding to carbonyl complexes of coordinatively unsaturated $Ce^{3+}$ cations (~2120-2130 $cm^{-1}$), $Ce^{4+}$ cations (~2160 $cm^{-1}$) and $Zr^{4+}$ cations (~2170-2180 $cm^{-1}$) are observed. The intensity of the strongest $Ce^{3+}$-CO complexes is rather low, although they appear after the first dose of CO, thus indicating their high bonding strength. At higher CO pressures in the gas phase (10 Torr), bands at ~ 2100 $cm^{-1}$ appear, which can be assigned to bicarbonyl complexes of $Ce^{3+}$ cations having at least two vacancies in their coordination sphere. Although $Ce^{3+}$ centers exist at the surface of a pure ceria sample prepared via OPCM, their density increases when Zr is introduced into the structure. This feature certainly correlates with the integral intensity of extended defects estimated by SAXS and enhanced absorption in the visible range of ceria-zirconia samples corresponding to bulk $Ce^{3+}$ cations (vide supra). Moreover, $Ce_{0.5}Zr_{0.5}O_x$ sample containing an admixture of zirconia-based phase (Table 1), although having a lower specific

surface area, has a higher intensity of bands in the 2100-2130 $cm^{-1}$ range. Hence, at least a part of surface coordinatively unsaturated $Ce^{3+}$ cations appears to be located at the interphase boundaries. Fluorination decreases the density of those centers probably due to incorporation of fluorine atoms into vacant positions in the coordination sphere of $Ce^{3+}$ cations. Simultaneously, as would be expected, the intensity of bands corresponding to carbonyls of $Ce^{4+}$ and $Zr^{4+}$ is increased (Fig. 2a, cf. spectra 2 and 3).

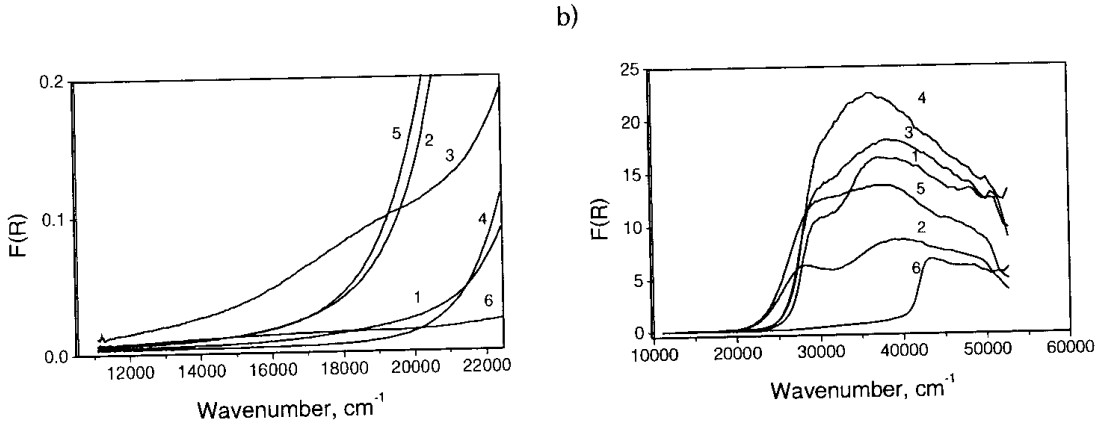


Fig. 1. UV-Vis spectra of the most homogeneous samples : 1 - $CeO_2$, 2 - $Ce_{0.8}Zr_{0.2}O_x$, 3 - $Ce_{0.6}Zr_{0.2}Ca_{0.2}O_x$, 4 - $Ce_{0.6}Zr_{0.2}Ca_{0.2}O_xF_y$, 5 - $Ce_{0.5}Zr_{0.5}O_x$, and 6 - $ZrO_2$.

Calcium addition removes the $Ce^{3+}$-CO band, decreases the intensity of the $Me^{4+}$-CO band, and shifts it to lower frequencies (cf. spectra 2 and 6, Fig. 2a). Since no appreciable variation in the density of bulk extended defects (Table 1) or Vis range absorption (Fig. 1) is observed, this result can be explained by preferential segregation of calcium cations in the vicinity of surface coordinatively unsaturated sites thus blocking them.

Estimation by using known values of carbonyls absorption coefficients [12] revealed that the surface density of $Ce^{3+}$ cations is less than 1% of a monolayer. Hence, those sites are clearly defects. For $Me^{4+}$ centers including weak ones filled only in the presence of gas phase CO, the integral surface density amounts up to 30-40 % of a monolayer, weakly depending on the sample nature. Hence, the predominant part of those sites can be assigned to 7-coordinated regular cations located on the most developed faces of the (111) type [13].

Pronounced variations with samples composition were also observed in the hydroxyls stretching region (Fig. 2c). For pure ceria sample, low-frequency bands corresponding to bridging hydroxyls bound with three cerium cations (~3638 $cm^{-1}$) as well as bulk hydrogen bound hydroxyls (band ~ 3570 $cm^{-1}$) dominate. A shoulder at ~3698 $cm^{-1}$ can be assigned to bridging hydroxyls bound with two $Ce^{4+}$ cations [14].

Incorporation of Zr shifts hydroxyl bands to higher frequency and makes them more intense. It implies that a part of the hydroxyls is bound with zirconium cations, since the hydroxyl band positions is rather close to those observed partially stabilized zirconias [15]. The appearance of bands at ~ 3780 $cm^{-1}$ implies the emergence of terminal hydroxyls. For

fluorine-containing sample, a band at ~ 3730 $cm^{-1}$ corresponding to terminal hydroxyls appears, due to fluorine incorporation into the coordination sphere of Ce cations. Calcium cations decrease the intensity of Brönsted acid sites as well due to surface sites blocking.

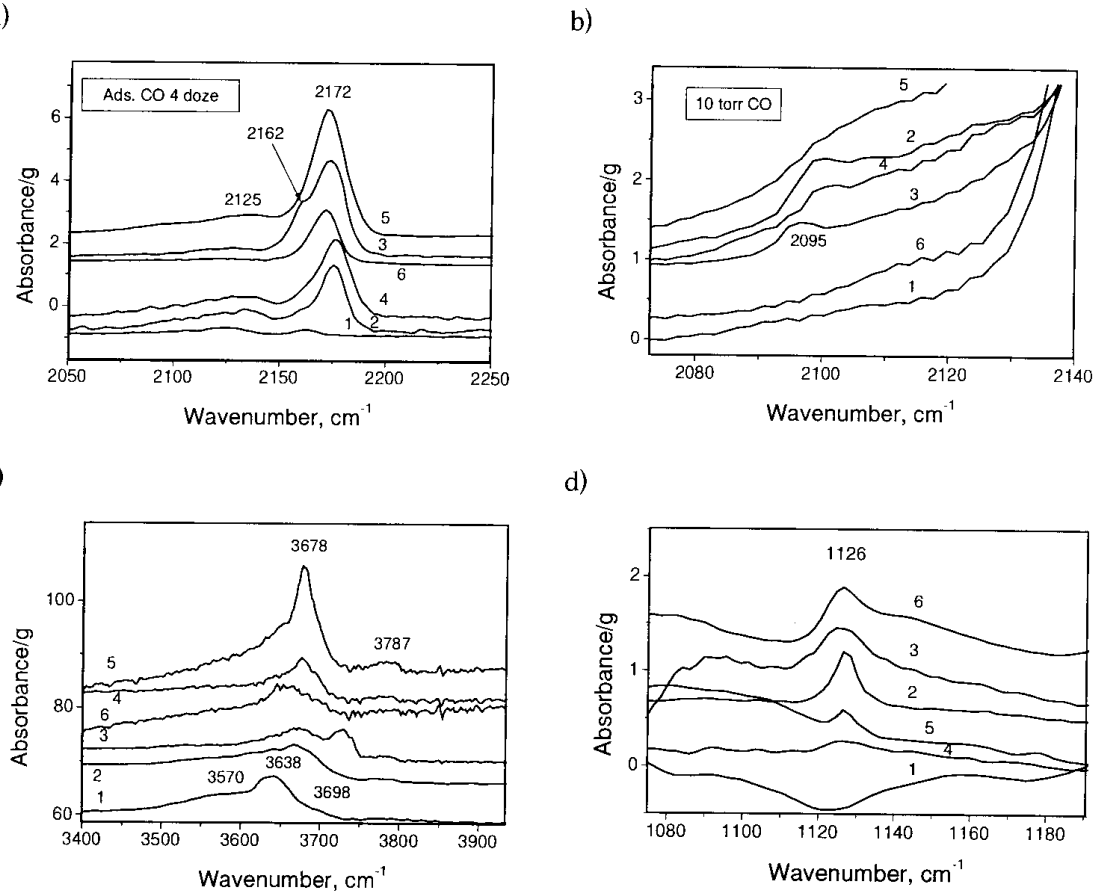


Fig.2 . FTIR spectra of adsorbed CO (carbonyl region) (a, b), OH groups ( c ) and adsorbed $O_2$ (d); Spectra designation: 1 - $CeO_2$ (sample 3), 2 - $Ce_{0.8}Zr_{0.2}O_x$ (sample 4), 3 - $Ce_{0.8}Zr_{0.2}O_xF_y$ (sample 9), 4 - $Ce_{0.5}Zr_{0.5}O_x$ (sample 10), 5 - $Ce_{0.5}Zr_{0.5}O_x$ (sample 11), 6 - $Ce_{0.6}Zr_{0.2}Ca_{0.2}O_x$ (sample 14).

As follows from Fig. 2d, contrarily to the pure ceria sample, samples of mixed fluorite-like solid solutions retain molecular forms of oxygen ($O_2^-$ [16]). The intensity of those bands is higher for samples containing calcium, fluorine and smaller amount of zirconium. It seems to correlate with the decreased ability of those systems to dissociate molecular oxygen due to a lower density of either highly unsaturated cations or clustered centers.

## 4. CONCLUSIONS

OPCM route of ceria—zirconia solid solutions synthesis appears to be reasonably flexible approach allowing to make rather broad substitution in cation and anion sublattices of fluorite-like oxides without appearance of new phases provided homogeneous mixing of starting salts is ensured. Reasonably high dispersion of samples thus obtained and disordered bulk and surface structure makes them promising candidates as catalysts and supports for red-ox reactions.

## ACKNOWLEDGMENTS.

This work is in part supported by RFBR/INTAS grant No IR—97-402.

## REFERENCES

1. M. Fathi, F. Monnet, Y. Schuurman, A. Holmen and C. Mirodatos, J. Catal., 190 (2000) 43.
2. J. Kaspar, P. Fornasiero and M. Graziani, Catal. Today, 50 (1999) 285.
3. M. Inoe, K. Sato, T. Nakamura and T. Inui, Catal. Lett., 65 (2000) 79.
4. S. Rossignol, F. Gerard and D. Duprez, J. Mater. Chem., 9 (1999) 1615.
5. M. Yashima, K. Ohtake, M. Kakihana and M. Yoshimura, J. Am. Ceram. Soc., 77 (1994) 2773.
6. V.A. Sadykov, S.F. Tikhov, G.N. Kryukova, N.N. Bulgakov, V.V. Popovskii and V.N. Kolomiichuk, J. Solid State Chem., 73 (1988) 200.
7. P. A. Cox, Transition Metal Oxides - An Introduction to their Electronic Structure and Properties, International Series of Monographs on Chemistry 27, Clarendon Press, Oxford, 1995.
8. G. Liu, J.A. Rodriguez, J. Hrbek, J. Dvorak, C.H.F. Peden and A.F. Rodriguez, J. Phys. Chem. B, 105 (2001) 7762.
9. C. Binet, A. Badri and J.C. Lavalley, J. Phys. Chem., 98 (1994) 6392
10. A. Emeline, G. Kataeva, A.S. Litke, A. Rudakova, V. Ryabchuk and N. Serpone, Langmuir, 14 (1998) 5011.
11. C.B. Azzoni and A. Paleari, Phys. Rev. B., 53 (1996) 53.
12. D.A. Seanor and C.H. Amberg, J. Chem. Phys., 42 (1965) 2967.
13. C. Conesa, Surf. Sci., 339 (1995) 337.
14. A.N. Kharlanov, E.V. Lunina and V.V. Lunin, Zh. Phyz. Khim., 71 (1997) 1672.
15. A.N. Kharlanov, E.V. Lunina and V.V. Lunin, Zh. Phyz. Khim., 73 (1999) 898.
16. M. Daturi, E. Finocchio, J-C. Lavalley, F. Fally, V. Perricon, H. Vidal, N. Hickey and J. Kaspar, J. Phys. Chem. B, 104 (2000) 9186.